

Huge quadratic magneto-optical Kerr effect in the Co_2FeSi Heusler compound

J. Hamrle, S. Blomeier, O. Gaier, B. Hillebrands

Fachbereich Physik and Forschungsschwerpunkt MINAS, Technische Universität Kaiserslautern, Erwin-Schrödinger-Straße 56, D-67663 Kaiserslautern, Germany

H. Schneider, G. Jakob

Institut für Physik, Johannes Gutenberg-Universität Mainz, Staudinger Weg 7, D-55128 Mainz, Germany

K. Postava

Department of Physics, Technical University of Ostrava, 17. listopadu 15, 708 33, Ostrava-Poruba, Czech Republic

C. Felser

Institute of Inorganic and Analytical Chemistry, Johannes Gutenberg-Universität Mainz, Staudingerweg 9, D-55128 Mainz, Germany

Abstract.

Co_2FeSi (CFS) films with L_{21} structure deposited on $\text{MgO}(001)$ were studied using longitudinal (LMOKE) and quadratic (QMOKE) magneto-optical Kerr effect. The films exhibit a huge QMOKE signal, with its maxima of up to 30 mdeg, which is the largest QMOKE signal in reflection that has been measured thus far. This is a fingerprint of an unusually large spin-orbit coupling of second or higher order. The CFS films exhibit a rather large coercivity of 350 or 70 Oe for CFS thicknesses of 22 or 98 nm, respectively. No angular dependence of the coercivity could be observed within the experimental error, despite the fact that the CFS films are epitaxial.

1. Introduction

Since its discovery by John Kerr in 1877 [1] the magneto-optical Kerr effect (MOKE) has evolved into a very powerful investigational tool for magnetic materials. In most cases only first order contributions of MOKE are detected, i.e. only the contributions proportional to the sample magnetization. In such a case (neglecting exchange bias systems), the measured MOKE loops are symmetric. The first order MOKE is historically divided into polar MOKE (PMOKE), proportional to out-of-plane magnetization, longitudinal MOKE (LMOKE), proportional to longitudinal magnetization and transverse MOKE (TMOKE), proportional to the magnetization component perpendicular to the plane of incidence. [2]

However, for some materials, for example Fe/MgO, [3], Fe/GaAs, [4], Fe/Ag, [5] and Py/Ta, [6] asymmetric MOKE loops were observed. Osgood *et al.* [7] and Postava *et al.* [3] first attributed the asymmetric nature of such loops to a superimposed quadratic MOKE (QMOKE) contribution, providing an even dependence on the applied magnetic field. Osgood *et al.* originally stated that the QMOKE is related only to the magnetization term $M_L M_T$, [7] and therefore concluded that QMOKE loops may only appear for systems where the magnetization reversal occurs by a coherent magnetization rotation, where M_L and M_T are the longitudinal and transverse magnetization components with respect to the plane of incidence, respectively. However, it has been shown that the QMOKE is proportional to two mixed terms, $M_L M_T$ and $M_L^2 - M_T^2$. [8] Hence the QMOKE loops may appear also in systems where magnetization reversal is driven by magnetic domains, as in the case of loops presented in this article.

The non-zero Kerr effect requires the presence of both spin-orbit (SO) coupling and exchange interactions. [9, 10] The first order MOKE (both PMOKE and LMOKE) originates from a component of \mathbf{M} parallel to \mathbf{k} , where \mathbf{k} is a wavevector of light *inside* the ferromagnetic materials. In this configuration, the first order contribution to SO coupling, $E_{\text{SO}} = \xi \mathbf{L} \cdot \mathbf{S}$, is dominant. [7] On the other hand, QMOKE originates from a component of \mathbf{M} perpendicular to the plane of incidence. In this configuration, the first order of SO coupling is zero, $\xi \mathbf{L} \cdot \mathbf{S} = 0$. Therefore, only SO coupling of second or higher order can give rise to QMOKE. As such higher order contributions of SO coupling are usually much smaller than those of first order, $\xi \mathbf{L} \cdot \mathbf{S}$, the QMOKE is usually much smaller than the first-order MOKE.

2. Longitudinal and quadratic MOKE

In order to facilitate the understanding of this work, we now briefly summarize the physical origin and theoretical description of both first order MOKE and QMOKE.

A cartesian coordinate system which will be used throughout this article is sketched in Fig. 1. The z -axis of this system corresponds to the sample out-of-plane axis, while the in-plane y - and x -axes are parallel and perpendicular to the plane of incidence, respectively. The sample orientation is described by an angle α , which is the angle

between the y -axis and the in-plane $[100]$ direction of the CFS crystal lattice. In the following, the relative sample magnetization components along the y and the x axis are called longitudinal M_L and transversal M_T magnetization, respectively. Note that the M_L and M_T components are defined with respect to the plane of incidence and not with respect to the orientation of the sample or with respect to the applied magnetic field.

The optical and magneto-optical properties of a magnetized crystal are described by the permittivity tensor ε_{ij} , which can be developed into a series in the components of the sample magnetization \mathbf{M} :

$$\varepsilon_{ij} = \varepsilon_{ij}^{(0)} + K_{ijk}M_k + G_{ijkl}M_kM_l + \dots, \quad (1)$$

where the M_i are the components of \mathbf{M} . In Eq. (1) the Einstein summation convention over the x , y , and z coordinates is used. The $\varepsilon_{ij}^{(0)}$, K_{ijk} and G_{ijkl} are constants, forming the dielectric tensor and the linear and quadratic magneto-optical tensors, respectively. [11] The number of independent components of these tensors can be reduced using the Onsager relation

$$\varepsilon_{ij}(\mathbf{M}) = \varepsilon_{ji}(-\mathbf{M}) \quad (2)$$

which can also be written in form of general symmetry arguments [11, 12]

$$\begin{aligned} \varepsilon_{ij}^{(0)} &= \varepsilon_{ji}^{(0)} \\ K_{ijk} &= -K_{jik}, \quad K_{iik} = 0 \\ G_{ijkl} &= G_{jikl} = G_{jilk} = G_{ijlk}. \end{aligned} \quad (3)$$

For cubic crystals (as in the case of CFS studied here), the number of independent tensor elements can be reduced further, resulting in only one free (complex) parameter in the constant term $\varepsilon_{ij}^{(0)}$, another one in the linear term K_{ijk} and three additional parameters in the quadratic term G_{ijkl} (note that the general symmetry relations determined by Eq. (3) are still valid) [12]

$$\begin{aligned} \varepsilon_{ij}^{(0)} &= \varepsilon_d \delta_{ij} \\ K_{ijk} &= K \\ G_{iiii} &= G_{11} \\ G_{iijj} &= G_{12}, \quad i \neq j \\ G_{1212} &= G_{1313} = G_{2323} = G_{44} \quad , \end{aligned} \quad (4)$$

with δ_{ij} being the Kronecker delta-function. Therefore, the off-diagonal elements of ε_{ij} can be written as (here we limit ourselves to in-plane magnetization only):

$$\begin{aligned} \varepsilon_{xy} &= \varepsilon_{yx} = 2G_{44}M_LM_T \\ \varepsilon_{xz} &= -\varepsilon_{zx} = KM_L \\ \varepsilon_{yz} &= -\varepsilon_{zy} = -KM_T \quad . \end{aligned} \quad (5)$$

On the other hand, at a sample orientation of $\alpha \neq 0$ the off-diagonal permittivity tensor elements can be written as

$$\varepsilon_{xy} = \varepsilon_{yx} = \left[2G_{44} + \frac{\Delta G}{2}(1 - \cos 4\alpha) \right] M_LM_T - \frac{\Delta G}{4} \sin 4\alpha (M_L^2 - M_T^2)$$

$$\begin{aligned}\varepsilon_{xz} &= -\varepsilon_{zx} = KM_L \\ \varepsilon_{yz} &= -\varepsilon_{zy} = -KM_T \quad ,\end{aligned}\tag{6}$$

by applying a rotational transformation around the z axis to the permittivity tensor ε_{ij} (see Refs. [12, 13]). In the above equation, $\Delta G = G_{11} - G_{12} - 2G_{44}$ denotes the so-called anisotropy parameter.

The relation between the Kerr effect $\Phi_{s/p} = \theta_{s/p} - i\epsilon_{s/p}$ and the permittivity tensor elements ε_{ij} was thoroughly studied in literature. [2, 14] $\theta_{s/p}$ and $\epsilon_{s/p}$ denote the Kerr rotation and Kerr ellipticity for s and p polarized incident light, respectively. A general analytical expression of the Kerr effect is too complicated for practical uses. Therefore two important analytical approximations for ultra-thin ferromagnetic layers or bulk-like ferromagnets are most often used, assuming either $t_{\text{FM}} \ll \lambda/4\pi N_{\text{FM}}$ or $t_{\text{FM}} \gg \lambda/4\pi N_{\text{FM}}$, respectively, with t_{FM} and N_{FM} being the thickness and the refractivity index of the FM layer. In both limiting cases, the analytical solution can be expressed as [15, 16, 17, 18]

$$\begin{aligned}\Phi_s &= -\frac{r_{ps}}{r_{ss}} = A_s \left(\varepsilon_{yx} - \frac{\varepsilon_{yz}\varepsilon_{zx}}{\varepsilon_d} \right) + B_s \varepsilon_{zx} \\ \Phi_p &= \frac{r_{sp}}{r_{pp}} = -A_p \left(\varepsilon_{xy} - \frac{\varepsilon_{xz}\varepsilon_{zy}}{\varepsilon_d} \right) + B_p \varepsilon_{xz}\end{aligned}\tag{7}$$

where the weighting optical factor $A_{s/p}$ ($B_{s/p}$) is even (odd) function of the angle of incidence φ . If ε_{ij} from Eq. (4) is substituted to Eq. (7), we obtain [8]

$$\begin{aligned}\Phi_{s/p} &= \pm A_{s/p} \left[2G_{44} + \frac{\Delta G}{2}(1 - \cos 4\alpha) + \frac{K^2}{\varepsilon_d} \right] M_L M_T \\ &\mp A_{s/p} \frac{\Delta G}{4} \sin 4\alpha (M_L^2 - M_T^2) \mp B_{s/p} K M_L,\end{aligned}\tag{8}$$

where $+$ ($-$) is related to the Kerr s (p) effect. Equation (8) is a final expression of the Kerr effect in case of an in-plane magnetized film with cubic symmetry. It shows several interesting features. (i) The last term, which is proportional to M_L , describes the ordinary LMOKE. (ii) There are two separate QMOKE contributions, being proportional to $M_L M_T$ and $M_L^2 - M_T^2$, respectively. (iii) The QMOKE depends on the crystallographic sample orientation α . (iv) Even if $G_{ijkl} \equiv 0$, there is a small quadratic contribution proportional to K^2 . It can be seen from Eq. (7) that this contribution originates from the mixed term $\varepsilon_{zx}\varepsilon_{yz}$ ($\varepsilon_{xz}\varepsilon_{zy}$) for Φ_s (Φ_p). This contribution is not due to an intrinsically quadratic dependence of ε_{ij} on the sample magnetization, but arises from a mixing of linear permittivity tensor components.

3. Sample properties and preparation

We have investigated the half-metallic Co_2FeSi (CFS) Heusler compound, which recently attracted lots of attention [19, 20, 21, 22, 23, 24, 25] as a possible candidate for spintronic applications. Up to now, CFS exhibits the highest observed magnetic moment ($5.97 \mu_B$) per formula unit (at 5 K, corresponding to an average value of $1.49 \mu_B$ per atom) and the highest Curie temperature (1100 K) among the so-called Heusler compounds and

half-metallic ferromagnets.[19] Our CFS films of thicknesses 11, 21, 42 and 98 nm were prepared by RF magnetron sputtering and deposited directly onto $\text{MgO}(001)$. The CFS films grow in the L2_1 ordered structure.[26, 27] All films were covered by a 4 nm thick Al protective layer. A detailed description of the sample preparation process as well as structural properties of such films can be found in Ref.[27].

4. Experimental loops

All Kerr measurements within this article were performed using s-polarized red laser light at a wavelength of $\lambda = 670$ nm. Typical Kerr rotation MOKE loops $\theta(H)$ measured on CFS(21 nm) are presented in Fig. 2. The topmost two loops in Fig. 2 were measured at an angle of incidence of $\varphi = 45^\circ$ and a sample orientation of $\alpha = \pm 22.5^\circ$. Both loops are asymmetric as they contain LMOKE (odd in H) and QMOKE (even in H) contributions. [3, 7] The loops' asymmetric nature changes sign when the sample orientation is changed from $\alpha = 22.5^\circ$ to -22.5° , corresponding to changes of sign of the QMOKE contribution. On the other hand, when the sample orientation is 0° or 45° (not shown in Fig. 2), the loops are symmetrical, which means that there is no QMOKE contribution in this case. These results are consistent with the expected fourfold symmetry of the QMOKE contribution [see Eq. (8)].

Any Kerr rotation loop can be separated into its symmetric θ_{sym} and antisymmetric θ_{asym} parts by using the relation: $\theta_{\text{sym/asym}} = [\theta_{\text{inc}}(H) \mp \theta_{\text{dec}}(-H)]/2$, where $\theta_{\text{inc/dec}}$ denotes the loop branch when H is increasing or decreasing, respectively. A more general way of the loop symmetrization and antisymmetrization valid also for systems with exchange bias have been presented by T. Mewes *et al.* [28]

The results of loop symmetrization and antisymmetrization are visualized in Fig. 2. The symmetrized (LMOKE) loops are identical for $\alpha = \pm 22.5^\circ$, so we show only one loop. Moreover, the antisymmetrized (QMOKE) loops differ only in sign in this case. Finally, the bottom loop (blue dash-dot line) shows the QMOKE loop as it is measured directly at a nearly normal angle of incidence of $\varphi \approx 0.5^\circ$ (for $\varphi = 0$, the LMOKE vanishes and hence the measured signal is proportional only to the QMOKE in the case of in-plane magnetized samples). As expected, the general shape of this QMOKE loop is identical to that of the QMOKE loops determined by antisymmetrization of the MOKE loops measured at $\varphi = 45^\circ$. However, the amplitude of the antisymmetrized QMOKE loop is slightly smaller, which can be attributed to a reduction of A_s when the angle of incidence increases [17].

5. Amplitude of QMOKE at saturation

In the previous section we have shown how to derive a QMOKE loop. However, it is also interesting to determine the value of the QMOKE signal at saturation. This parameter is an analog of the the LMOKE signal at saturation which is experimentally determined (in the case of Kerr rotation, for example) as $\theta_{\text{sat}, M_L} = [\theta(H_{\text{sat}}) - \theta(-H_{\text{sat}})]/2$, where

H_{sat} is the saturation field of the sample. The QMOKE signal at saturation can also be determined, but in a more complicated way, [8] where the Kerr signal is subsequently measured after application of an external field in eight different directions \mathbf{H}_1 to \mathbf{H}_8 (Fig. 1(b)), which is sufficient to saturate the sample each time. In this case, [see Eq. (8)], the LMOKE Kerr rotation signal at saturation is $\theta_{\text{sat}, M_L} = [\theta(\mathbf{H}_8) - \theta(\mathbf{H}_4)]/2$, while the QMOKE signal at saturation proportional to $M_L M_T$ and $M_L^2 - M_T^2$ write

$$\theta_{\text{sat}, M_L M_T} = [\theta(\mathbf{H}_1) + \theta(\mathbf{H}_5) - \theta(\mathbf{H}_3) - \theta(\mathbf{H}_7)]/4 \quad (9)$$

$$\theta_{\text{sat}, M_L^2 - M_T^2} = [\theta(\mathbf{H}_8) + \theta(\mathbf{H}_4) - \theta(\mathbf{H}_2) - \theta(\mathbf{H}_6)]/4. \quad (10)$$

Figure 3 displays the angular dependence of the different MOKE signals at saturations of the CFS(21 nm) sample at an angle of incidence of $\varphi = 0.5^\circ$. Points determined by the 8-directional method described above are represented by full symbols. In agreement with Eq. (8), we obtain the result that the LMOKE signal is independent on α (\blacksquare). The QMOKE signal related to $M_L^2 - M_T^2$ is proportional to $\sin(4\alpha)$ (\blacktriangle) whereas the QMOKE signal related to $M_L M_T$ is proportional to $\cos(4\alpha) + \text{const}$ (\bullet). The absolute vertical shift in the angular dependence of $M_L M_T$ is proportional to G_{44} [see Eq. (8)] whereas the amplitudes of both sinusoidal graphs are proportional to the anisotropy term ΔG .

Experimental data in Fig. 3 provides the same amplitude for both sinusoidal graphs. On the other hand, theory (Eq. (8)) predicts that the sinusoidal amplitude proportional to $M_L M_T$ should be twice large compared to the amplitude proportional to $M_L^2 - M_T^2$. When external magnetic field is applied, for example, in \mathbf{H}_1 direction, then $M_L = M_T = 1/\sqrt{2}$, assuming saturation magnetization being 1. Then, $M_L M_T = 1/2$, which reduces the QMOKE amplitude related to $M_L M_T$ by a factor of 2. Therefore, the discrepancy in the QMOKE amplitudes in Fig. 3 and Eq. (8) comes from the determination of the experimental QMOKE signal proportional to $M_L M_T$, as given by Eq. (9). In this equation, the linear combination of Kerr signals should be divided by a factor of 2 instead of 4. However, we keep definition as given in Eqs. (9-10) from historical reasons. [8, 12]

Finally it can be noted that for the CFS(21 nm) sample (see Fig. 3), the QMOKE amplitude is 20 mdeg and the maximal QMOKE signal reaches 30 mdeg. To our knowledge, those values are the highest QMOKE amplitude and signal in reflection that have ever been measured.

6. Peak heights in QMOKE loops

We measured QMOKE loops in the directions of \mathbf{H}_1 to \mathbf{H}_8 for different sample orientations α . Figure 4 shows such an example of a QMOKE loop determined for CFS(21 nm) at $\alpha = -22.5^\circ$, when the positive magnetic field was applied in \mathbf{H}_8 direction, i.e., in y -direction. The linear slope in the QMOKE loops originates from a Faraday effect arising in optical elements of the setup due to the stray field of the magnet used in the experiments. The large full circle (\bullet) at $H = 0$ shows the QMOKE signal in

saturation, as determined in the previous Section. The value of the signal consequently determines the absolute value of Kerr rotation in the QMOKE loop. It shows that the QMOKE loop has its maxima at sample saturation. As the magnetic field is reduced from saturation, the QMOKE signal decreases and finally reaches zero value at the top of the peaks (i.e., at a field of H_c). Consequently, it holds that $\langle M_L M_T \rangle = 0$ and $\langle M_L^2 - M_T^2 \rangle = 0$ simultaneously during reversal, i.e., at $H = H_c$, where $\langle \dots \rangle$ indicates that these values are averaged over the laser spot area (which has a diameter of $\approx 300 \mu\text{m}$). This fact shows that the reversal process occurs by the nucleation and growth of magnetic domains. In case of coherent magnetization reversal, the average values $\langle M_L M_T \rangle$ and $\langle M_L^2 - M_T^2 \rangle$ cannot be equal to zero simultaneously. The presence of magnetic domains during the reversal process is also confirmed by LMOKE loops measured at $\varphi = 45^\circ$, where the magnetic field was applied in transverse (x) direction and no LMOKE signal was obtained.

To check whether all QMOKE loops provide zero value at $H = H_c$, we determined the height of the peaks for loops measured at different α and at $\mathbf{H}_1 \dots \mathbf{H}_8$ directions of applied magnetic field. The determination of the peak heights is sketched in Fig. 4. The values of peak heights are then processed by the 8-directional method. The results obtained by this method are represented by open symbols in Fig. 3. It can be seen that for any α , QMOKE signal determined from peak heights and related to $M_L M_T$, $M_L^2 - M_T^2$ have the same value as those determined at saturation. It shows that for any α , the QMOKE loops are always reaching their zero value during reversal at $H = H_c$. Therefore the reversal is always provided through magnetic domains, where $\langle M_L M_T \rangle = 0$ and $\langle M_L^2 - M_T^2 \rangle = 0$.

7. Coercive field

Figure 5 displays a polar plot of the coercive field H_c as determined from LMOKE symmetrized loops for CFS(21 nm) sample. H_c is constant within experimental error (which is about 1.5% in our case). This constant nature of H_c has been observed for all studied thicknesses of CFS films. Furthermore, this constant nature of coercivity was also observed for CFS films irradiated with different fluences of Ga^+ ions. [29]

The constant nature of H_c is very surprising, as our CFS samples are epitaxial and therefore one should naively expect the presence of hard and easy axes. However, such hard and easy axes may still be present in our samples because, as have been shown in Sec. 6, the magnetization reversal occurs by domain wall propagation. Moreover, the shape of LMOKE symmetrized loops is also independent on α . Hence, our CFS samples are unique examples of an epitaxial system, where the switching field along the hard and easy axis direction is balanced, resulting in a coercive field that is constant with the sample orientation α .

8. Dependence on film thickness

Figure 6 shows Kerr rotation hysteresis loops determined for different film thicknesses t_{CFS} at two different sample orientations $\alpha = \pm 22.5^\circ$. It can be observed that the hysteresis loops become more and more squared with increasing t_{CFS} while H_c is decreasing. This can most likely be attributed to an improvement of the crystalline quality of the films with increasing thickness, which leads to a higher mobility of domains walls. The reduction of H_c with t_{CFS} is shown quantitatively in Fig. 7(a). For this purpose, the value of H_c was determined from symmetrized LMOKE loops, as the QMOKE contribution effectively reduces the coercivity (see Sec. 5). Figure. 7(a) shows that a change of t_{CFS} from 21 nm to 98 nm results in a reduction of H_c by almost a factor of 5, i.e., from 345 Oe down to 70 Oe.

Figure 7(b) shows the dependence of different MOKE signals on t_{CFS} . We present the Kerr rotation θ , the Kerr ellipticity ϵ , as well as their Pythagorean average $\Omega = \sqrt{\theta^2 + \epsilon^2}$ for both LMOKE and QMOKE signals. Here, the QMOKE signal was determined from peak heights obtained from measurements recorded at angle of incidence $\varphi = 45^\circ$ and sample orientation $\alpha = 22.5^\circ$. It can be observed that the LMOKE signal (\blacktriangle) saturates at high thicknesses whereas the QMOKE signal (\triangle) reaches a maximum at an intermediate thickness and then decreases again. In order to better understand this behavior, we also measured the Kerr ellipticity in both cases, which exhibits a similar, but opposite behavior: the LMOKE Kerr ellipticity (\blacksquare) reaches a maximum and then decreases again whereas the QMOKE Kerr ellipticity (\square) monotonically increases with increasing thickness.

Such a behavior can be attributed to the depth sensitivity of the magneto-optical Kerr effect.[2, 15, 30] This is clearly demonstrated for the Pythagorean average Ω of both the LMOKE and QMOKE signals (full and empty stars in Fig. 7). With increasing t_{CFS} , both LMOKE and QMOKE Pythagorean averages reach their maxima at t_{CFS} near 20-30 nm and then saturate to some value with further increasing thickness.

In particular, the Kerr effect originating from an ultrathin sublayer of thickness Δt situated at a depth t_i can be expressed as

$$\Phi_i \approx C \Delta t \exp \left[\frac{4i\pi t_i N_{z,\text{CFS}}}{\lambda} \right], \quad (11)$$

where $N_{z,\text{CFS}} = \sqrt{(N_{\text{CFS}}^2 - N_{\text{air}}^2 \sin^2 \varphi)}$ is the normalized (complex) k -vector in z -direction, N_{air} is the refractivity index of air and C is a complex constant.[2, 15, 30] The resulting Kerr effect Φ_{tot} is given by summation over all contributions originating from different depths, $\Phi_{\text{tot}} = \sum_i \Phi_i$. Due to the exponential term in Eq. (11), a Kerr signal originating from a deeper sublayer t_i exhibits a larger damping as well as a larger shift in phase. The Kerr signals originating from different depths t_i and t_j differ by a phase (Eq. 11) $\Delta\zeta_{i-j} = 4\pi\Re(N_{z,\text{CFS}})(t_i - t_j)/\lambda$. If the ferromagnetic films are thick and transparent enough, as in our case, then the Kerr effects Φ_i , Φ_j from depths t_i , t_j may differ by a phase π . In such a case, Φ_i and Φ_j cancel each other, leading to a

reduction of the resulting Kerr effect, in agreement with the behavior of Pythagorean average $\Omega = |\Phi_{\text{tot}}|$ in Fig. 7.

In conclusion, the dependencies of both Kerr rotation and ellipticity on the CFS film thickness seem to be determined by phenomenological optical and magneto-optical properties of the investigated samples and not by a change of their electronic structures.

9. Summary

Co_2FeSi (CFS) films in the L_{21} structure of thicknesses 11–98 nm and deposited onto $\text{MgO}(001)$ were studied by means of the longitudinal (LMOKE) and quadratic (QMOKE) magneto-optical Kerr effect. The samples exhibit a huge QMOKE effect with amplitude of 20 mdeg and the maximum QMOKE signal reaching 30 mdeg at a sample thickness of 21 nm. To our knowledge, those are the highest values of QMOKE amplitude and signal in reflection that has been measured so far. Furthermore, it is a fingerprint of an unusually large spin-orbit coupling of second or higher order in CFS. Although the samples are epitaxial, they do not show an angular dependence of the coercivity as well as the shape of LMOKE loops within an experimental error of 1.5%. The samples exhibit rather large coercivities of 350 or 70 Oe for CFS thicknesses of 21 or 98 nm, respectively. The magnetization switching occurs through magnetic domains. When the magnetic field during reversal reaches $H = H_c$, then averaging over many magnetic domains results in $\langle M_L M_T \rangle = 0$ and $\langle M_L^2 - M_T^2 \rangle = 0$ for any sample orientation α . The thickness dependence of the obtained LMOKE and QMOKE signals was found to be consistent with a phenomenological magneto-optical description. Therefore, a thickness dependence of the electronic structure of the investigated CFS films could be excluded.

10. Acknowledgment

The project was financially supported by the Research Unit 559 "New materials with high spin polarization" funded by the Deutsche Forschungsgemeinschaft, and by the Stiftung Rheinland-Pfalz für Innovation. Partial support from the Grant Agency of the Czech Republic (202/06/0531) is acknowledged. We would like to thank T. Mewes for stimulating discussions.

- [1] Kerr J 1877 *Philos. Mag.* **3** 321
- [2] Hubert A, Schäfer R. Magnetic Domains: The Analysis of Magnetic Microstructures. Berlin: Springer-Verlag; 1998
- [3] Postava K, Jaffres H, Schuhl A, Nguyen Van Dau F, Goiran M, Fert AR 1997 *J. Magn. Magn. Mater.* **172** 199
- [4] Yan SS, Schreiber R, Grünberg P, Schäfer R 2000 *J. Magn. Magn. Mater.* **210** 309
- [5] Cowburn RP, Ferré J, Jamet JP, Gray SJ, Bland JAC 1997 *Phys. Rev. B* **55** 11593
- [6] Mattheis R, Quednau G 1999 *J. Magn. Magn. Mater.* **205** 143
- [7] Osgood III RM, Bader SD, Clemens BM, White RL, Matsuyama H 1998 *J. Magn. Magn. Mater.* **182** 297
- [8] Postava K, Hrabovský D, Pištora J, Fert AR, Višňovský Š, Yamaguchi T 2002 *J. Appl. Phys.* **91** 7293
- [9] Hulme HR 1932 *Proc. R. Soc. London* **A135** 237
- [10] Bruno P, Suzuki Y, Chappert C 1996 *Phys. Rev. B* **53** 9214
- [11] Višňovský Š 1986 *Czech. J. Phys. B* **36** 625
- [12] Postava K, Pištora J, Yamaguchi T, Hlubina P. Polarized light in structures with magnetic ordering. In: Pluta M, Szyjer M, Powichrowska E, editors. Lightmetry 2002: Metrology and Testing Techniques Using Light vol. 5064 of Proc. of SPIE Bellingham, Wash.: SPIE; 2003. p. 182–190
- [13] Višňovský Š 1986 *Czech. J. Phys. B* **36** 1424
- [14] Zvezdin AK, Kotov VA. Modern Magnetooptics and Magneto-optical Materials. London: Taylor & Francis; 1997
- [15] Traeger G, Wenzel L, Hubert A 1992 *Phys. Stat. Sol. (a)* **131** 201
- [16] Qiu Z, Bader S 1999 *J. Magn. Magn. Mater.* **200** 664
- [17] Višňovský Š, Nývlt M, Prosser V, Lopusník R, Urban R, Ferré J, Pénissard G, Renard D, Krishnan R 1995 *Phys. Rev. B* **52**(2) 1090
- [18] Hamrle J, Ferré J, Jamet JP, Repain V, Baudot G, Rousset S 2003 *Phys. Rev. B* **67**(15) 155411
- [19] Wurmehl S, Fecher GH, Kandpal HC, Ksenofontov V, Felser C, Lin HJ 2006 *Appl. Phys. Lett.* **88** 032503
- [20] Inomata K, Okamura S, Miyazaki A, Kikuchi M, Tezuka N, Wojcik M, Jedryka E 2006 *J. Phys. D: Appl. Phys.* **39** 816
- [21] Kallmayer M, Elmers HJ, Balke B, Wurmehl S, Emmerling F, Fecher GH, Felser C 2006 *J. Phys. D: Appl. Phys.* **39** 786
- [22] Kandpal HC, Fecher GH, Felser C, Schönhense G 2006 *Phys. Rev. B* **73** 094422
- [23] Hashimoto M, Herfort J, Schönherr HP, Ploog KH 2006 *Appl. Phys. Lett.* **87** 102506
- [24] Wurmehl S, Fecher GH, Kandpal HC, Ksenofontov V, Felser C, Lin HJ, Morais J 2005 *Phys. Rev. B* **72** 184434
- [25] Niculescu V, Budnick JI, Hines WA, Raj K, Pickart S, Skalski S 1979 *Phys. Rev. B* **19** 452
- [26] Wurmehl S, Fecher GH, Kroth K, Kronast F, Dürr HA, Takeda Y, Saitoh Y, Kobayashi K, Lin HJ, Schönhense G, Felser C 2006 *J. Phys. D: Appl. Phys.* **39** 803
- [27] Schneider H, Jakob G, Kallmayer M, Elmers HJ, Cinchetti M, Balke B, Wurmehl S, Felser C, Aeschlimann M, Adrian H 2006 arXiv:cond-mat/0606666
- [28] Mewes T, Nembach H, Rickart M, Hillebrands B 2004 *J. Appl. Phys.* **95** 5324
- [29] Hamrle J, Blomeier S, Gaier O, Reuscher B, Brodyanski A, Kopnarski M, Postava K, Schneider H, Jakob G, Felser C, Hillebrands B 2006 arXiv:cond-mat/0609633. To be published
- [30] Hamrle J, Ferré J, Nývlt M, Višňovský v 2002 *Phys. Rev. B* **66**(22) 224423

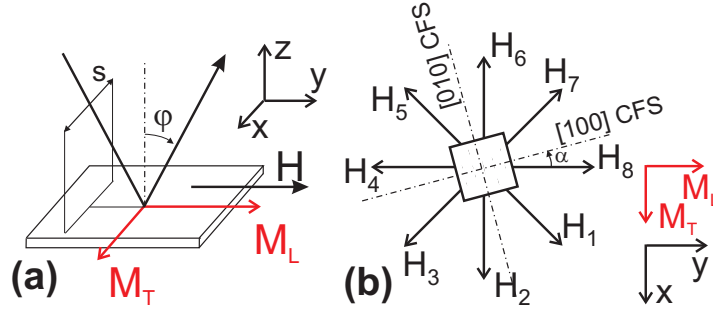


Figure 1. (color online) (a) Sketch of the sample and the incident s-polarized light. (b) Definition of the 8 directions of the externally applied magnetic field which are used to determine the values of the QMOKE signal in saturation. α denotes the sample orientation, i.e., the angle between the $[100]$ CFS direction and the plane of incidence of the incoming light (y -axis).

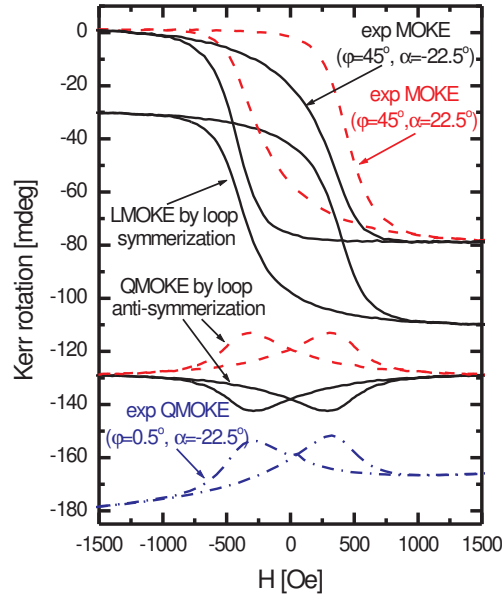


Figure 2. (color online) MOKE loops recorded from the CFS(21 nm) sample. The topmost two loops were directly measured at $\phi = 45^\circ$ and $\alpha = 22.5^\circ$ (red dashed line) or $\alpha = -22.5^\circ$ (black full line), respectively. These two loops are symmetrized and anti-symmetrized (see text for details), providing LMOKE and QMOKE contributions. The bottom loop (blue dash-dotted line) is a QMOKE loop directly measured at $\phi = 0.5^\circ$ and $\alpha = -22.5^\circ$.

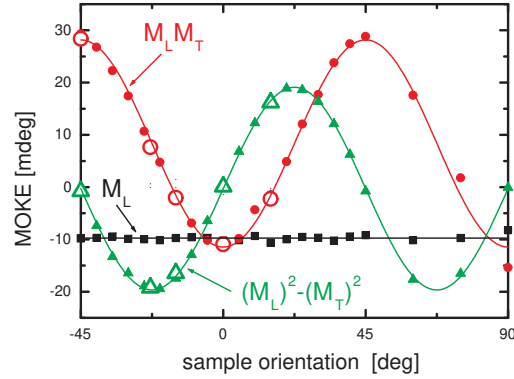


Figure 3. (color online) (full symbols) Dependence of different MOKE signals at saturation for the CFS(21 nm) sample on the sample orientation α at $\varphi = 0.5^\circ$, which are determined from the 8-directional method [8]. (open symbols) MOKE signals determined from the height of peaks in QMOKE loops. See text for details.

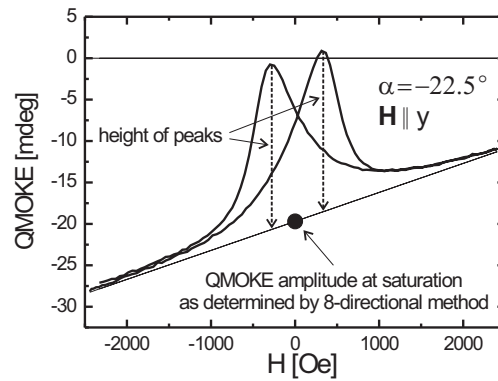


Figure 4. QMOKE Kerr rotation loop in CFS(21 nm) measured at $\varphi = 0.5^\circ$, at a sample orientation $\alpha = -22.5^\circ$, and within positive field ranges applied in y direction. The full circle at $H = 0$ shows the QMOKE signal at saturation as determined by the 8-directional method for this particular α . Dashed arrows illustrate how the height of the peaks in the QMOKE loop is determined. It can be seen that the QMOKE is at maximum when the sample is in saturation. Furthermore, the QMOKE is zero when the peaks are reaching their highest signal.

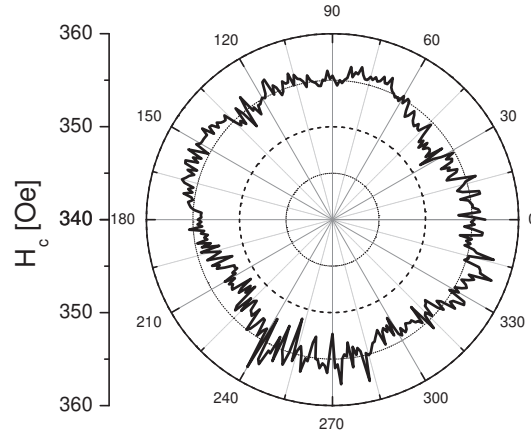


Figure 5. Dependence of the coercive field on the sample orientation α as determined from symmetrized LMOKE loops in CFS(21 nm) sample.

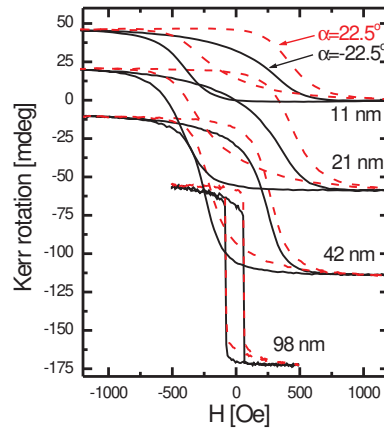


Figure 6. (color online) MOKE hysteresis loops for different thicknesses of CFS films, recorded at an angle of incidence $\varphi = 45^\circ$. The sample orientation is equal to 22.5° (dashed red line) or -22.5° (full black line).

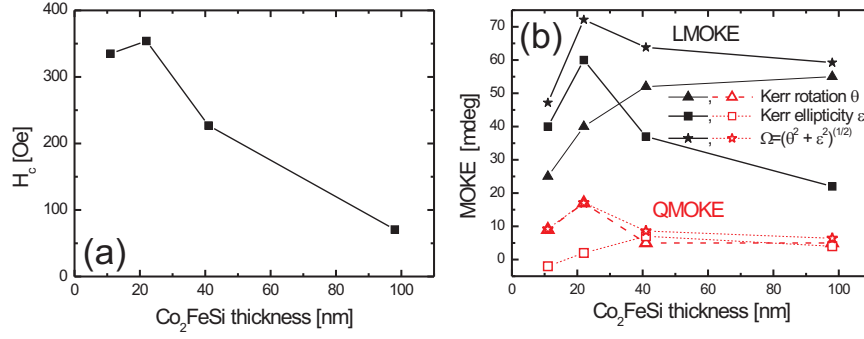


Figure 7. (color online) Dependence of (a) H_c as well as (b) the LMOKE and QMOKE signals at saturation on the film thickness, measured at $\varphi = 45^\circ$. The QMOKE signal was determined from the height of peaks in QMOKE loops, which are obtained by antisymmetrization of experimental MOKE loops.